

Simulation of the power transmission of bone-conducted sound in a finite-element model of the human head

You Chang¹  · Namkeun Kim²  · Stefan Stenfelt¹ 

Received: 11 July 2017 / Accepted: 7 July 2018 / Published online: 17 July 2018
© The Author(s) 2018

Abstract

Bone conduction (BC) sound is the perception of sound transmitted in the skull bones and surrounding tissues. To better understand BC sound perception and the interaction with surrounding tissues, the power transmission of BC sound is investigated in a three-dimensional finite-element model of a whole human head. BC sound transmission was simulated in the FE model and the power dissipation as well as the power flow following a mechanical vibration at the mastoid process behind the ear was analyzed. The results of the simulations show that the skull bone (comprises the cortical bone and diploë) has the highest BC power flow and thereby provide most power transmission for BC sound. The soft tissues was the second most important media for BC sound power transmission, while the least BC power transmission is through the brain and the surrounding cerebrospinal fluid (CSF) inside the cranial vault. The vibrations transmitted in the skull are mainly concentrated at the skull base when the stimulation is at the mastoid. Other vibration transmission pathways of importance are located at the occipital bone at the posterior side of the head while the transmission of sound power through the face, forehead and vertex is minor. The power flow between the skull bone and skull interior indicate that some BC power is transmitted to and from the skull interior but the transmission of sound power through the brain seem to be minimal and only local to the brain–bone interface.

Keywords Bone conduction sound · Finite-element model · Power transmission

1 Introduction

Bone-conducted (BC) sound produces an auditory sensation when vibrations stimulate the inner ear via mechanisms different from ordinary air conduction (AC) transmission through the ear canal and middle ear (Stenfelt and Goode 2005b). Even if BC sound is transmitted in the bone of the skull, the outer and middle ear may contribute to the final auditory perception (Stenfelt et al. 2002; Stenfelt et al. 2003). However, the main distinction between AC and BC sound is that BC sound has a dominant sound power transmission through the skull bone (Eeg-Olofsson et al. 2008; Stenfelt and Goode 2005a; Eeg-Olofsson et al. 2013), the soft tissues, or the interior of the skull (Sim et al. 2016; Roosli et al. 2016).

Hearing by BC is usually described as sound power transmitted through the body (Stenfelt 2013). But the exact pathways conveying the sound power have not been clarified. For example, with BC stimulation at the mastoid, the sound transmission to the contralateral ear can be transmitted through the thin bony shell of the cranial vault, through the thicker skull base, or as a sound pressure through the interior of the skull. Therefore, an investigation of the sound power transmission could result in a better understanding of BC hearing in the human. However, vibratory power transmission in a living human or a cadaver head is difficult to measure. One possible solution is to compute the power transmission using a simulation model for BC sound.

Recently, a three-dimensional finite-element (FE) model of the whole human head was developed by Chang et al. (2016). The model was reconstructed from the anatomy of an adult female head through the Visible Human Project© (<http://vhnet.nlm.nih.gov/>). The dynamic response of the whole head FE model was validated by comparing the simulation results with the experimental data obtained in cadaver heads and living humans (Eeg-Olofsson et al. 2008; Eeg-Olofsson et al. 2011; Håkansson et al. 1986; Stenfelt

✉ You Chang
chang.you@liu.se

¹ Department of Clinical and Experimental Medicine, Linköping University, Linköping, Sweden

² Department of Mechanical Engineering, Incheon National University, Incheon, Korea

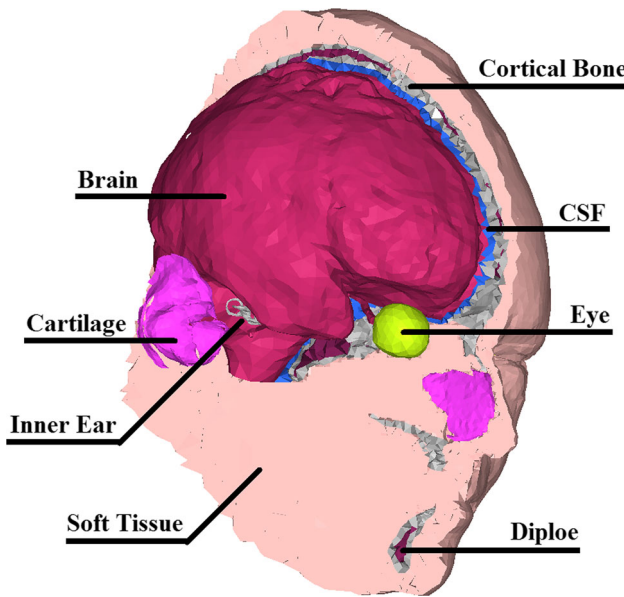


Fig. 1 An illustration of the FE model LiUHead with its components. Details of the model and components are described in the text

and Goode 2005a). The simulated BC sound transmission in that model was similar to average data from several datasets of BC experiments. As a result, that model could be used to estimate BC power transmission in a human head.

In the current study, this 3D FE model of the whole human head was simulated in the frequency domain with the aim to compute the BC power flow and the dissipated power. The main goal is to investigate the role of the different head-structures and tissues in the power transmission, and to determine dominant BC power transmission pathways for BC sound in the human head by analyzing the distribution of BC sound power flow.

2 Materials and methods

2.1 Finite-element model

The details of the FE model of the whole human head, hereafter referred to as LiUHead, can be found in Chang et al. (2016) and only an overview of the FE model is given here. The geometry of the LiUHead is based on an adult female and the FE model consists of 87,000 nodes and 481,000 tetrahedron elements (each with 4 nodes). The LiUHead comprises eight domains: (1) the brain (2) cerebrospinal fluid (CSF) (3) eye balls, (4) inner ears, (5) cartilages, (6) cortical bone (including teeth), (7) soft bone (diploë), and (8) soft tissues (including skin, muscles, and connective tissues) (Fig. 1). One unique feature with the LiUHead is the 3-layer sandwich design of the skull bone similar to real skull–bone where soft spongy bone (diploë) is interposed between inner and outer

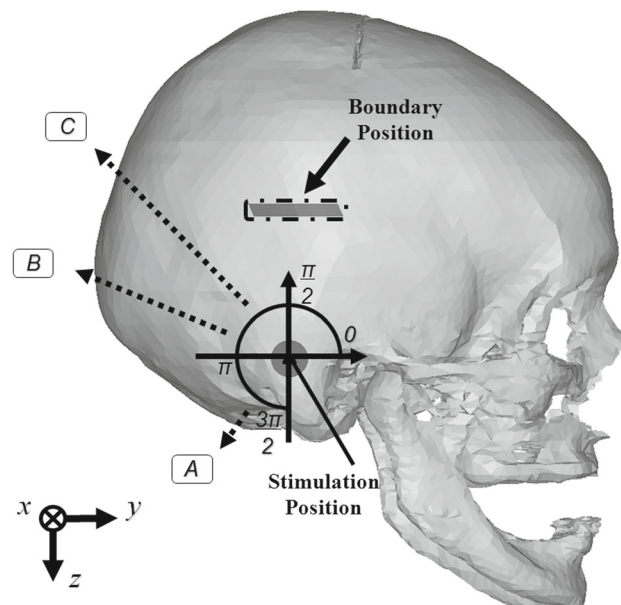


Fig. 2 Ipsilateral view of the skull bone. The three perpendicular directions are indicated as well as the stimulation position at the mastoid. A circle around the stimulation position was used to determine the measurement locations and pathway directions where the direction in the positive y-direction was defined as 0 rad. The three dotted lines indicate the three pathways A, B, C described in the text. The gray area superior to the stimulation position shows the area for computation of sound power exchange between the skull bone and skull interior and the gray area around the stimulation position is the area for the same computations including the stimulation position

layers of dense cortical bone. The excitation is provided at the mastoid skull bone using a triangular prism shaped mass to simulate a screw implanted through the outer layer of the cortical bone and the diploë similar to stimulations with bone anchored hearing aids (BAHA) (Berger 1976; Mudry and Tjellström 2011). The parameter values for the eight domains were obtained from the literature and are provided in Chang et al. (2016).

2.2 Simulation setup

The dynamic behavior of the LiUHead was computed by the FE solver COMSOL Multiphysics® (COMSOL Inc., Stockholm, Sweden) in the frequency range from 0.1 to 10 kHz. The frequency resolution was 25 Hz in the range of 100–500, 50 Hz in the range of 500–1000 and 100 Hz in the range of 1–10 kHz. Three orthogonal directions were defined for the vibratory calculations where x is the direction from the stimulation side toward the middle of the head (medial), y is the direction toward the front of the head (anterior), and z is the direction toward the bottom of the head (inferior) (Fig. 2). The stimulation was applied as a dynamic force on the screw with a magnitude of 1 N. The stimulation direction was perpendicular to the surface of the skull with a vector of (0.98,

0.03, 0.17). The head is assumed symmetrical about the mid-line and the stimulation was only applied on one side of the LiUHead. The head model was setup as a free boundary as in Chang et al. (2016).

2.2.1 Power flow

To investigate the power flow of BC sound in the human head, a simulation of sound power was computed using the LiUHead. The eight domains of the LiUHead were grouped into three different structures to ease computations and interpretations. The three parts were: (1) the soft tissue and cartilages located outside of the skull bone, (2) the skull bone comprising two layers of cortical bone interposed with one layer of diploë, and (3) the brain and CSF including the eye balls and inner ear fluids, located inside the skull bone.

Since a sinusoidal stimulation was applied on the surface of the triangular prism shaped screw in the frequency domain, the total power input applied to the whole head system is calculated as:

$$P_{\text{inp}} = \frac{1}{2} \text{real}(\mathbb{F} \cdot \mathbb{V}^*) \quad (1)$$

which is the half of the real part of the applied complex force \mathbb{F} multiplied with the complex conjugate of the resulting complex velocity \mathbb{V} of the stimulation surface (input velocity). The simulation was computed in the frequency domain and the power flow was obtained from the FE solver. Based on COMSOL Multiphysics®, the power flow into an element of the model is defined as:

$$P_D = \frac{1}{2} \text{real}(\boldsymbol{\sigma} \cdot (\boldsymbol{i}\omega\boldsymbol{\varepsilon})) \quad (2)$$

which is the half of the real part of the stress tensor $\boldsymbol{\sigma}$ multiplied by the strain tensor $\boldsymbol{\varepsilon}$ times the angular frequency (ω) and the imaginary unit i . The stress tensor $\boldsymbol{\sigma}$ is defined as the pressure acting on an area and the strain tensor $\boldsymbol{\varepsilon}$ is the deformation of the geometry that is material specific. Accordingly, the P_D is the dissipated power of each element. It should be noted in this context that the simulation is in a free boundary condition meaning that the values outside the boundary are equal to zero (Lee 1980). This implies that during the simulations no sound radiation into the surrounding air occurs and the input power should equal the sum of dissipated power in the structures, according to the law of energy conservation (Hambric 1990).

The BC power flow, or mechanical power flux, is computed in COMSOL as the half of the real part of the stress

tensor multiplied by the complex conjugate of the complex velocity:

$$\begin{bmatrix} P_{Fx} \\ P_{Fy} \\ P_{Fz} \end{bmatrix} = -\frac{1}{2} \text{real} \left(\begin{bmatrix} \sigma_{xx} & \sigma_{xy} & \sigma_{xz} \\ \sigma_{xy} & \sigma_{yy} & \sigma_{yz} \\ \sigma_{xz} & \sigma_{yz} & \sigma_{zz} \end{bmatrix} \cdot \begin{bmatrix} v_x^* \\ v_y^* \\ v_z^* \end{bmatrix} \right) \quad (3)$$

Here, P_{Fx} , P_{Fy} , and P_{Fz} are the power flow through a unit area in the x -, y -, and z -directions, respectively. The power flow defined in this way has the unit kg/s^3 . The minus sign means that if a pressure is applied on an external area, and it moves in the direction of the load, then a positive power input in the direction of the load is obtained. The power flow can be understood as the mechanical energy transmitted per second through a unit area. Equation 2 describes the general definition of power flow, while Eq. 3 is the specific calculation for a given infinitesimal volume.

2.2.2 Directions of the transcranial transmission in the skull bone

As stated previously, the skull bone is often assumed as the important medium for BC sound transmission. But the way the sound is transmitted in the bone is not well understood. This was investigated here by computing the sound power transmitted in the skull bone radially from the stimulation position. This analysis was conducted by first creating an artificial circle with approximately 20 mm radius around the stimulus position on the skull bone, illustrated in Fig. 2. This circle only served to define the radial direction from the stimulation position to a point on the circle. On this circle, 14 measurement positions were identified and the directions between the stimulation positions and the measurement positions indicate the transmission direction where the direction along the positive y -axis was defined as 0 degrees. Due to the anatomy of the skull, the ring of measurement positions did not form a complete circle and the measurement positions ranged from 0.12 to 4.01 rad (approximately 7°–230°), corresponding to approximately 2/3 of the circle.

The bone thickness at each measurement position differs and the thickness of each layer (two layers of cortical bone and one layer of diploë) was recorded. The width for each pathway was defined as 1 mm. In this way, an area was defined of each bone layer that was 1 mm (the width) times the thickness of each layer and perpendicular to the direction between the stimulation position and the measurement point. The power flow through this defined area was then computed as the power flow in-line with the transmission direction integrated over the area for each position on the imaginary circle in Fig. 2.

The simulation was computed in the frequency domain and the power flow P_F was computed according to Eq. 3

above. Then the power flow in the direction vector of the unit area orthogonal to the pathway was computed as:

$$P_{F_Pathway} = P_{Fx} \cdot \vec{a}_x + P_{Fy} \cdot \vec{a}_y + P_{Fz} \cdot \vec{a}_z \quad (4)$$

where P_{Fi} is the component of the power flow in the i direction and \vec{a}_i is the direction vector of the area orthogonal to the pathway in the i direction.

From the computation of Eq. 4, the radial directions with the greatest BC sound power transmission were identified. These directions were used to investigate the sound power transmission from the ipsilateral side of the skull to a position corresponding to the stimulation position on the contralateral side. For each measurement position, the skull bone thickness was estimated and an area derived (the thickness multiplied by 1 mm) and the power flow through this area derived as explained above. This investigation of sound power transmission was accomplished by computing the area and the power flow according to Eq. 4 in line with the radial directions, here termed pathways, at positions spaced about 9.5 mm apart along each half circumference connecting the stimulation position and a mirrored location on the contralateral side. There are 15, 19 and 25 measurement positions for pathways A, B and C, respectively.

2.2.3 Sound transmission through the skull interior

One possible pathway not investigated in the analysis of radially transmitted power is the sound power transmitted through the skull interior. For transcranial transmission, the direction through the skull interior is the shortest pathway from the ipsilateral side to the contralateral side of the head and require transmission of sound power from the skull bone to the fluid and neural tissue inside the cranium, and back to vibration in the skull bone at the contralateral side. To investigate the power transfer between the skull bone and skull interior, two boundaries between the inner layer of the skull bone and the brain/CSF on both sides were selected. The aim here is to investigate the interaction between the skull bone and the skull interior.

The boundaries investigated were randomly selected in the widest region of the skull. However, the boundaries were chosen to not include the stimulation position. The rationale for this was that the forced excitation at the stimulation position causes local skull bone deformation that is different from the vibrational response at positions away from the stimulation position. The boundaries were also chosen to be located at similar positions at both sides with similar areas. The boundaries used in the current study were about 50 mm superior to the stimulation position, marked as the gray area surrounded by a dashed-dotted line in Fig. 2. The outward power flow, which is defined as the scalar product of the 3D power flow (Eq. 3) and the normal vector of the

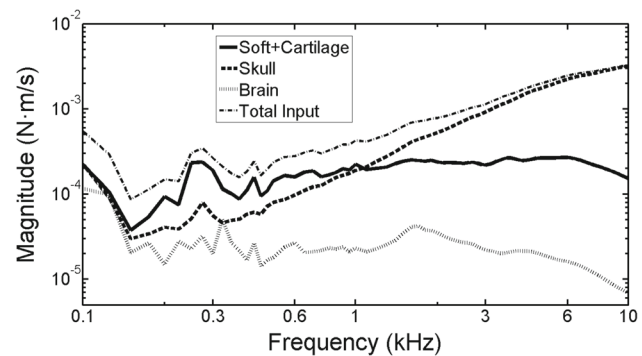


Fig. 3 The power dissipation in the three parts of the head as: the soft tissues (solid line), the skull bone (dashed line), and the brain with CSF (dotted line). The total input power is shown as the thin dashed-dotted line

measured boundaries, was used to investigate the BC sound power transmitted through the skull interior.

In addition to the boundaries presented above, the power transmission between the skull bone and the skull interior at the stimulation position was calculated. This was accomplished by identifying an approximately circular area of 10 mm in diameter with centered around the stimulation position, shown as the gray area around the stimulation position in Fig. 2. The power flow through this boundary was computed similar to that described above.

3 Results

3.1 Power dissipation

The BC powers dissipated in the three structures of the head are shown in Fig. 3 where the power in the soft tissue and cartilages is shown with a solid line, in the skull bone with a dashed line, and in the brain with a dotted line. The stimulation is a dynamic force of 1 N at the side of the skull (see Fig. 2) at all frequencies and the total input power is displayed with a thin dashed-dotted line in Fig. 3. The dissipated power decreases with frequency at the lowest frequencies for all structures but increases above 150 Hz for the skull bone and soft tissues while it is relatively constant for the skull interior. The power dissipated in the soft tissue and cartilages is greatest among the three structures and close to the total input power up to about 1 kHz, and then stays approximately constant. The power dissipated in the skull bone shows similar tendency as the total input power and the magnitude is the highest among all three structures at frequencies above approximately 1 kHz. The power dissipated in the brain show a tendency similar with the power dissipated in the soft tissue, but around one order of magnitude lower.

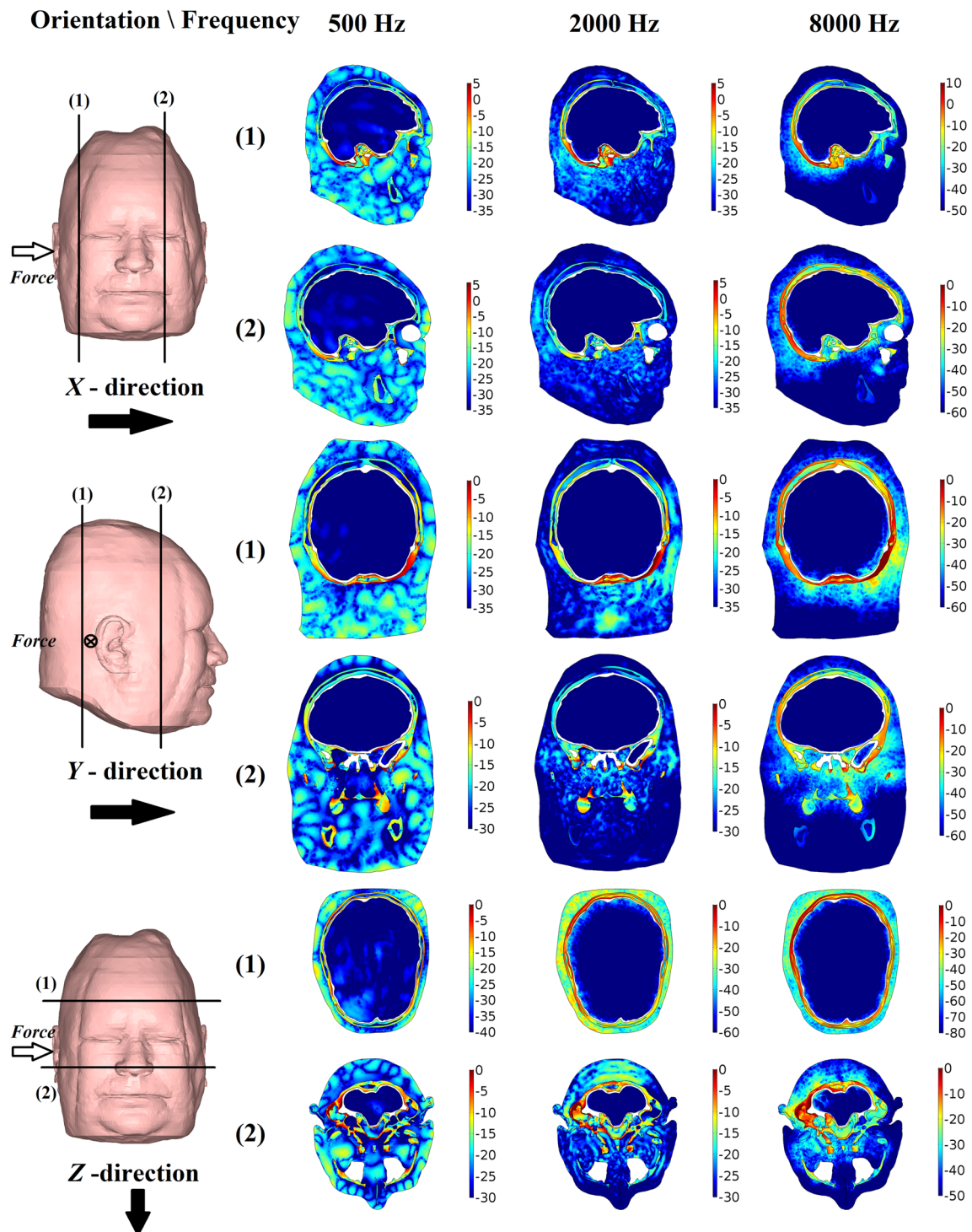


Fig. 4 The power flow in the head shown at three frequencies (0.5, 2 and 8 kHz). The power flow is shown for two cross sections (1 and 2) for each direction separately and the direction is into the cross-sectional surface. The level of power flow is color coded and the color bars show the level for each cross section in dB re 1 N/(ms). For the *x*-direction, the

stimulation position is anterior to the cross sections, for the *y*-direction, the stimulation position is on the right-hand side of the cross sections, and for the *z*-directions, the stimulation position is on the left hand side of the cross sections

3.2 Power flow in the head

The power flow, calculated according to Eq. 3, is the BC power that flows through a unit area in a specified direction. To grasp the BC power flow in the human head the power flow in the three directions are illustrated in Fig. 4 for each direction at two cross sections of the head and at three frequencies, 500, 2, and 8 kHz. For each direction, two cross sections are defined and the power flow magnitudes in line with the direction are color-coded. For example, the top row of Fig. 4 shows the power flow in the x -direction (toward the midline) at around 50 mm lateral to the midline. At 500 Hz, the greatest power flow is at the lower parts of the skull bone, the skull base and occipital bone area (yellow–red), while the soft tissues and cranial bone indicate less power flow (green–light blue) and the brain tissues show the least power flow (dark blue). At the higher frequencies, 2 and 8 kHz, the highest power flow is still in the skull base and occipital bone area and the rest of the skull bone show greater power flow (green) than the soft tissues (light blue–blue) and the brain tissue (dark blue).

The same tendencies are seen at the other directions in Fig. 4 and the associated cross-sectional views, the bones in the skull base show 10–30 dB greater power flow than the cranial vault, and the skull bone indicates a 10–20 dB greater power flow than the soft tissues at 500 Hz that increases to 30–60 dB at 8 kHz. Figure 4 also shows a relatively evenly distribution of the power flow in the soft tissue at the low frequencies (500 Hz), while it is significantly greater close to the skull bone than far from the skull bone at the high frequencies (8 kHz).

The brain tissue shows the least power flow at all directions, cross sections, and frequencies. Compared to the skull base power flow, the power flow in the brain is 30–40 dB lower at 500 Hz and 50–60 dB lower at 8 kHz. This result indicates that the brain tissue is insignificant for BC power flow.

3.3 Power transmission in the bony medium of the skull

The radially transmitted power in the skull bone, computed as the power flow, obtained at the 14 measurement positions on the circle around the stimulation position according to Fig. 2 and the corresponding area at the measurement position were analyzed in 3 frequency bands in Fig. 5: (1) low frequencies (from 100 to 600 Hz, solid line), (2) mid-frequencies (from 600 to 3 kHz, dashed line), and (3) high frequencies (from 3 to 10 kHz, dotted line). The radially transmitted power in the skull bone in Fig. 5 is shown as the average power flow for each frequency band (defined as the sum of the power flows in each frequency band divided by the number of frequencies) as a function of the measurement position (angle on the

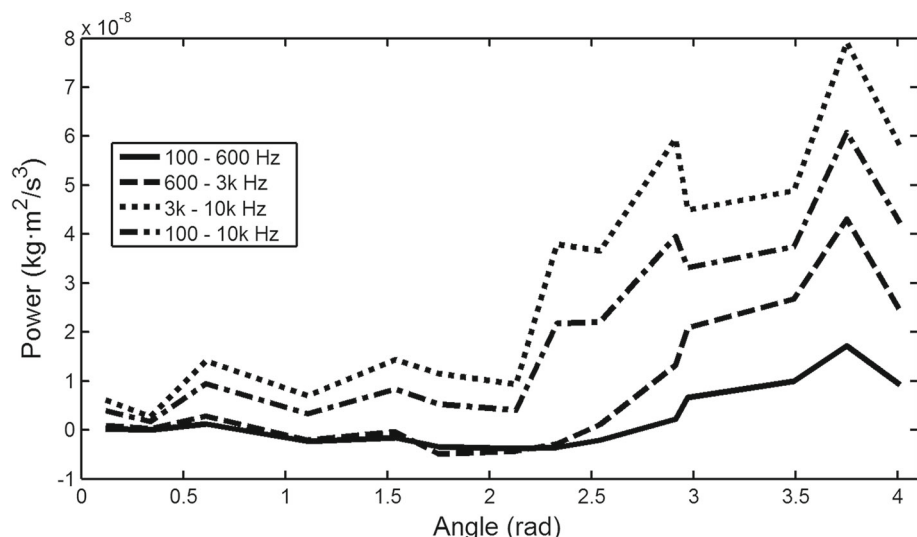
circle). It should be noted that the directions of the radially transmitted powers are defined as the x , y , and z components that constitutes the vector from the stimulation position to the measurement position on the circle. In addition to the averaged transmitted power in the three frequency bands in Fig. 5, the mean transmitted power for the whole frequency range is shown as a dashed-dotted line.

The general trend is that for a 1 N stimulation at the mastoid bone, most power transmission in the skull bone is at the highest frequencies and along directions with an angle above 2.3 rad. It should also be noted that at the low frequencies, and at some directions also at the mid-frequencies, the average power is negative (for low frequencies between 0.8 and 2.7 rad). This means that at those frequencies and at those directions, the power is directed toward the stimulation position. This finding is here interpreted as a result of the near rigid motion at low frequencies (Stenfelt and Goode 2005a, b). At these frequencies, a large part of the motion is composed of three-dimensional translational and rotational motion of the entire skull. With the stimulation position as in the current simulations, a rotational motion of the head is induced causing a net displacement toward the stimulation position for directions toward the vertex (1.57 rad). At higher frequencies, where wave motion in the skull bone is present (Stenfelt and Goode 2005a, b; Dobrev et al. 2017), the power is in the direction radially out from the stimulation positions (positive values the dotted line in Fig. 5).

The powers at all four frequency ranges in Fig. 5 have a maximum at the measurement position at 3.75 rad. Moreover, a local maximum is seen for the whole frequency range at 2.91 rad and another local maximum is found at 2.33 rad. These three directions are further investigated to reveal the power transmission in transcranial BC sound transmission in the skull bone.

Those three radial pathways were denoted A (3.75 rad), B (2.91 rad) and C (2.33 rad) according to their decreasing magnitudes (Fig. 2). The pathway with the maximum power transmission (A) was at the skull base, passing close to the foramen magnum. The other two are at the rear part of the skull bone where pathway B was over the occipital bone and pathway C was on the border between the occipital and parietal bones. It is not suggested here that these three pathway directions are solely responsible for BC transmission in humans, but they serve as examples of BC power transmission over the skull bone. For example, Fig. 5 indicates that directions in the 2.91–4 rad range have significantly greater radially power transmission than directions below 2.2 rad. This suggests the majority of BC sound power is transmitted in the bone in the skull base and lower back (occiput) of the skull and only a fraction of the BC power is transmitted over the vertex or forehead, which is also consistent with the power flow plots in Fig. 4.

Fig. 5 The power flow in the skull bone through the unit areas at the 14 measurement positions around the stimulation point as a function of the angle in radians. Zero radians means the direction to the forehead and π radians is the direction to the back of the head. Three frequency regions are shown: low frequencies (from 100 to 600 Hz, solid line), mid-frequencies (from 600 to 3 kHz, dashed line), and high frequencies (from 3 to 10 kHz, dotted line). The dashed-dotted line is the mean values of the whole frequency range



Positions interspersed by approximately 9.5 mm were defined along the directions of the three defined pathways, between the ipsilateral stimulation position and the corresponding position at the contralateral side. At those points, the component of the transmitted power in the skull bone in the direction of the pathway was computed according to Eq. 4. Pathway A had a total distance of about 140 mm and comprised 15 measurement positions, pathway B had a total distance of around 188 mm and comprised 19 measurement positions, and pathway C had a total distance of 234 mm and comprised 25 measurement positions. The transmitted power computed for each pathway was divided into frequency regions of low, mid, and high frequencies as in Fig. 5. In Fig. 6, the mean skull bone transmitted powers are displayed for each frequency region in the upper panel and the area for which the powers are estimated in the lower panel. The reason for the variation in area with distance is the variation of the skull thickness.

While the skull bone thickness oscillates irregularly with distance (Fig. 6), there is an overall trend of reduced skull bone power transmission with distance at all frequency ranges. In pathway A, all frequency ranges showed positive values at all distances. This was not the case for pathways B and C which had negative values at some position for the low and mid-frequencies. In pathway B, negative values were seen for the low frequencies at distances above 50 mm and for the mid-frequencies at distances above 140 mm. In pathway C, the transmitted power has negative values at the low frequencies for more or less the entire distance, while the negative values for the mid-frequencies were found at distances above 150 mm. The high frequencies had positive values for the entire distance at all three pathways. The high frequencies had the greatest magnitude reduction of transmitted skull bone power with distance where the reduction between the two sides was around 2 orders of magnitude.

The mid-frequencies had less magnitude loss with distance, while the transmitted skull bone powers at the low frequencies showed the least magnitude effect with distance.

In Figs. 5 and 6, the transmitted power in the skull bone is computed in the radial direction according to the defined pathway. However, as indicated in Fig. 4, the skull bone power is transmitted in the directions orthogonal to this direction as well. For example, if power in the skull bone is transmitted to or from the skull interior or the surrounding soft tissues, it would not be captured by the computations in Figs. 5 or 6. To investigate how much of the transmitted skull bone power that was in line with the pathway and how much was in other directions, the transmitted skull bone power was computed in all three dimensions for the three defined pathways. This power, here termed the overall transmitted power in the skull bone, is computed as the sum of the absolute value of the transmitted power in the all three dimensions. In Fig. 7, the two transmitted powers are shown for the three pathways where the transmitted power in the direction of the pathway is shown with a solid line and the overall transmitted power computed in all three space dimensions is shown with a dashed line. Those two transmitted powers in the skull bone are the average values computed as the sum the transmitted powers for all frequencies simulated and divided by the number of frequencies. The overall transmitted power in the skull bone decreases with distance in pathways A and B where the decrease in pathway B slows down after 100 mm, approximately at the rear of the skull. Pathway C shows the same decrease with distance as in pathways A and B up to around 125 mm, where it becomes near constant independent of distance. Compared with the transmitted skull bone power in the direction of the pathway, the overall transmitted power in the skull bone has higher magnitude and less steep slope. The difference between the overall transmitted power and the transmitted power in the direction of the pathway is

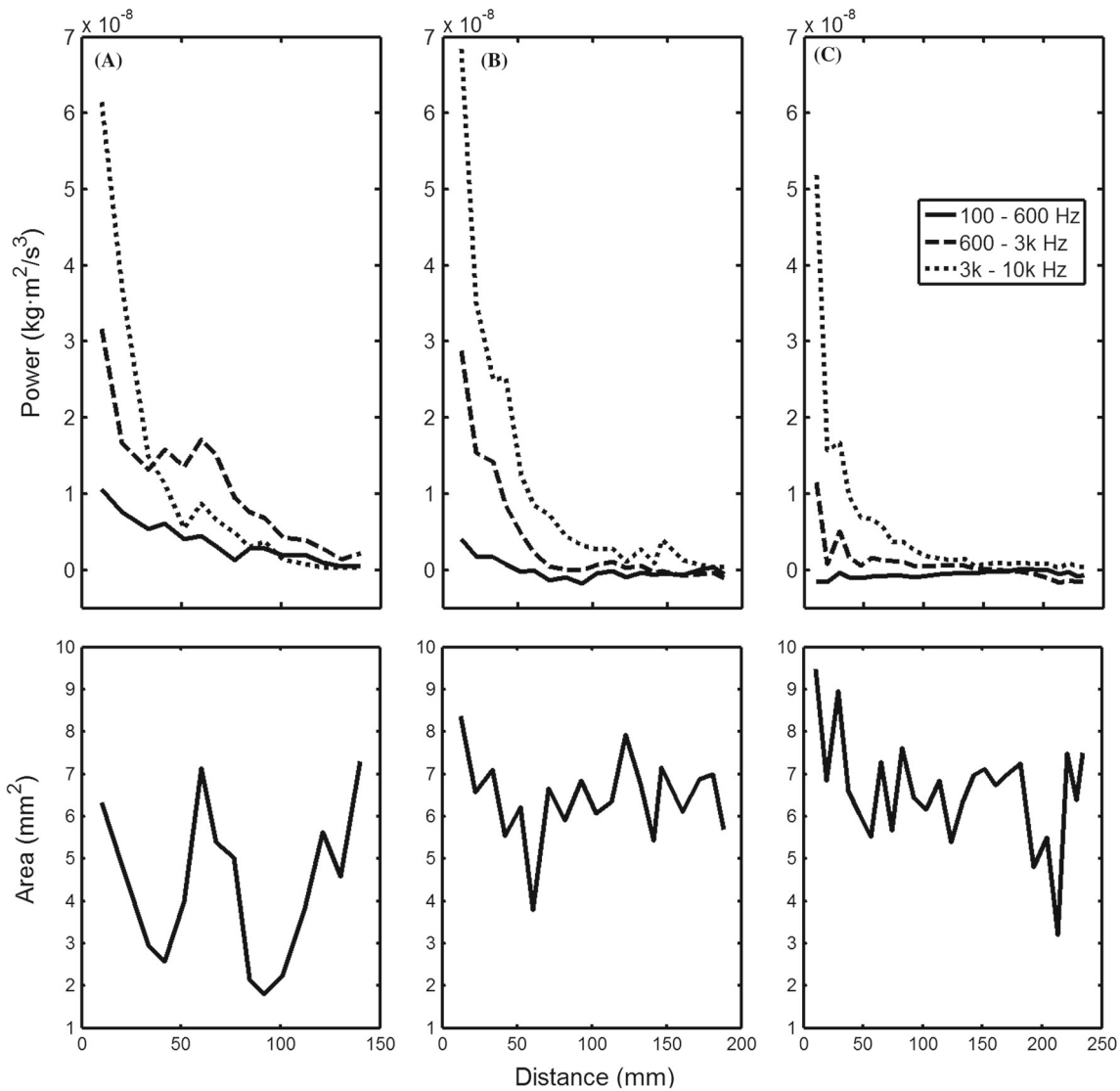


Fig. 6 The skull bone power transmitted in line with the three pathways, *A*, *B* and *C* (upper panels) and the area used to estimate the transmitted power (lower panels). The *x*-axis shows the distance on the skull

bone surface between the measurement positions and the stimulation position. The curves show the mean values for low-, mid-, and high-frequency ranges similar as in Fig. 5

about 0.1 order of magnitude near the stimulation position but increases to between 0.5 and 1.5 order of magnitude at the opposite side. This means that at close to the stimulation position, most of the transmitted power is in line with the radial direction in the skull bone, but far from the stimulation position, especially on the contralateral side, the major part of the transmitted power in the skull bone is at directions orthogonal to the pathway directions (as defined here) or a mixture of positive and negative transmitted power over the frequency range in the pathway direction.

3.4 Power flow transmission through the skull interior

The BC sound interaction between the skull bone and the skull interior was determined by computing the outward power flow in COMSOL between the skull and CSF/Brain tissue at both ipsilateral and contralateral sides. The outward power flow function computes the power flow (Eq. 3) in the normal direction of an area. The direction from the skull bone to the skull interior was defined as positive at the ipsilateral side of the stimulation position, while the direction from the brain and CSF to the skull bone was positive at the contralateral side. This means that the direction from the ipsilateral toward the contralateral side is positive at both sides. The

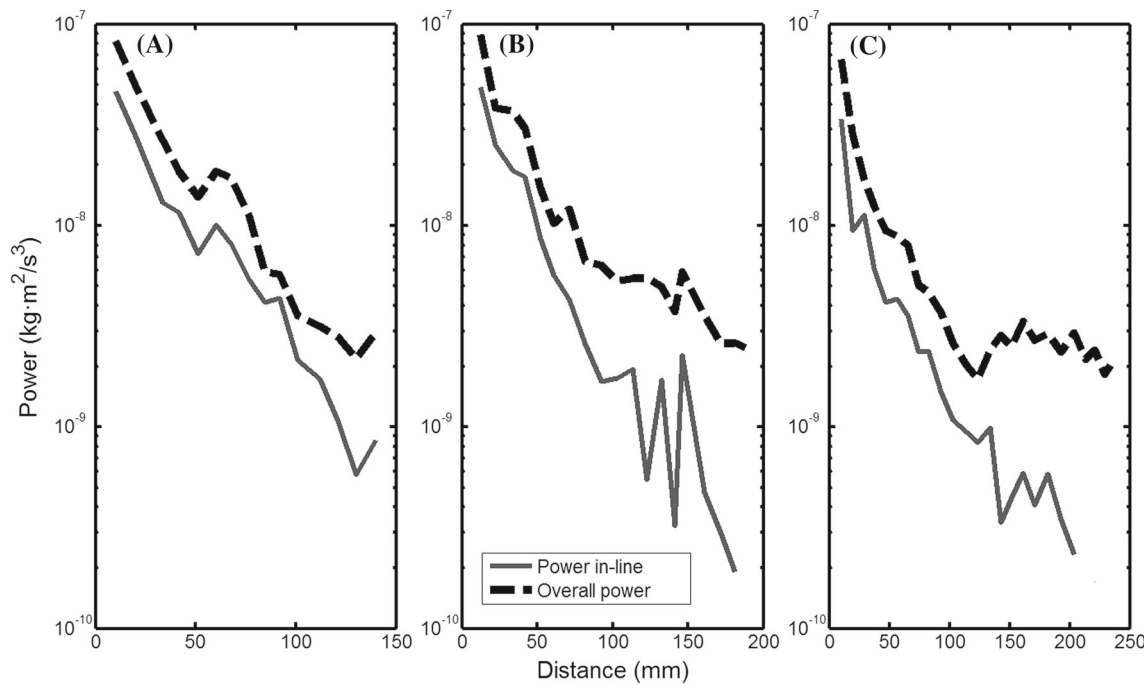
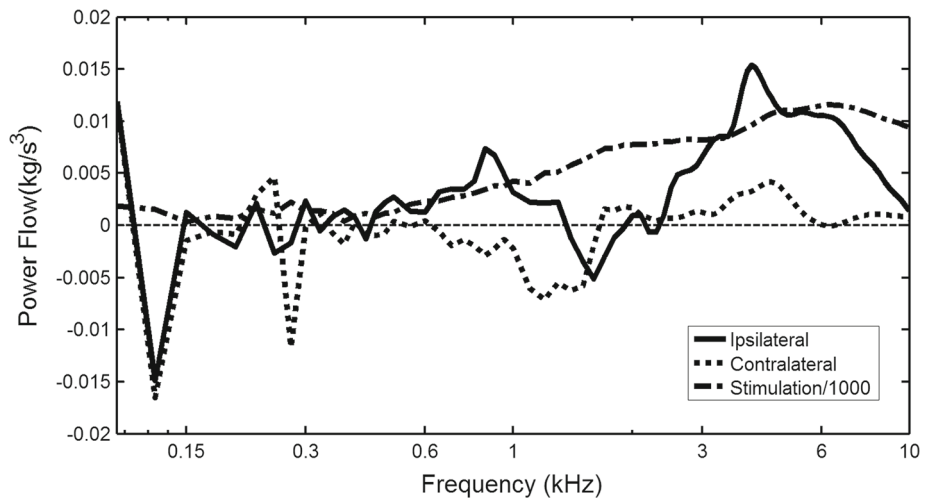


Fig. 7 The overall power transmitted in the skull bone in the three pathways A, B and C (dashed line) and the skull bone power transmission in-line with the three pathway directions (solid line). The curves are average values for the entire frequency range of 0.1–10 kHz

Fig. 8 The power flow through the boundaries defined in Fig. 2 between the skull bone and the brain and CSF. At the ipsilateral side, the power flow transmitted to the skull interior is shown with a solid line while the power flow transmitted from the brain and CSF to the skull bone at the contralateral side is shown with a dotted line. The thin dashed line indicates the zero level, which means no power flow transfer between the two parts. The dashed-dotted line indicates the power flow through the boundary including the stimulation position. This power flow is here divided by 1000 to have a magnitude similar to the other power flows



outward power flow is averaged over the whole boundary area at each side. The computed outward power flow at the ipsilateral side is shown with a solid line in Fig. 8 and at the contralateral side with a dotted line. The dashed line at zero indicates no power exchange between the skull bone and the skull interior while a positive value indicates a power flow toward the contralateral side and a negative value means a power flow toward the ipsilateral side.

As shown in Fig. 8, at the ipsilateral side, the power flow is positive in the mid-frequency range (between 500 and

1200 Hz) and at high frequencies (above 2.5 kHz), indicating that at these frequencies, the vibratory power flow is from the skull bone to the skull interior. At the other frequencies, the results are close to 0 except at around 130 and 1.5 kHz, where the power flow is in the direction from the skull interior to the skull bone. Consequently, at these frequencies, vibratory power travel from the skull interior to the skull bone at the investigated area on the ipsilateral side.

At the contralateral side, there is a negative peak at 130 and 280 Hz; otherwise, the vibratory power interchange is close

to zero up to 600 Hz. Between 0.6 and 1.8 kHz, the power flow is negative meaning that vibratory power transmission is from the skull bone to the skull interior. At frequencies above 1.8 kHz and up to 10 kHz, the power flow is positive and vibratory power is transferred from the skull interior to the skull bone. Consequently, no clear trend is visible at the lowest frequencies, but at frequencies approximately between 0.6 and 1.5 kHz, vibratory power is transmitted from the skull bone into the skull interior at both the ipsilateral and contralateral sides, while at high frequencies, above 2.5 kHz, part of the vibratory power seem to be transmitted from the ipsilateral skull bone through the skull interior and back to the contralateral skull bone.

The power flow through the boundary around the stimulation position, averaged over the area, is shown as the dashed-dotted line in Fig. 8. The result was significantly greater than the power flows at the other boundaries and was reduced 1000 times to be in the same range as the other power flows in Fig. 8. This clearly indicates that around the stimulation position, there is a significant power transmission from the skull bone into the brain tissue.

To investigate the power transmission through the skull interior further, a pathway parallel to the x -axis (the shortest distance) was defined between the center of the ipsilateral boundary and the center of the contralateral boundary. In a way similar to the power computations in Fig. 6, the power through the skull interior in the direction of the x -axis was computed as the power flow in the pathway from the ipsilateral boundary to the contralateral boundary over an area of $1 \text{ mm} \times 1 \text{ mm}$ at the boundary between the skull bone and CSF, in the CSF, and at distances of 12.5 mm in the brain tissue. The power flow in the skull interior according to this computation is shown in Fig. 9a.

If the power transmission direction in Fig. 9a is in the x -direction (from the ipsilateral to the contralateral side), it is indicated with thick lines and if the transmission direction is opposite to the x -direction (from the contralateral to the ipsilateral side) it is indicated with thin lines. The power transmitted through the brain shown in Fig. 9a is in the x -direction (shows positive values) at the ipsilateral side at all three frequency ranges. For the low and mid-frequencies, the power transmission is in the x -direction to about the middle, while the high frequencies show transmission in the opposite direction already after 25 mm into the brain. There is no clear trend at further distances for the high frequencies that alternately indicate transmission in the x -direction and opposite direction. At the furthest points, at the contralateral side, both the low and the high frequencies show positive values indicating a power transmission toward the contralateral skull bone at these points in line with the data in Fig. 8. It is also noticeable that there is a great loss of power transmission of 1–2 orders of magnitude from the position at the skull bone border to just a few millimeters inside the brain tissue. It is

also clear that the brain tissue does not transmit BC sound power at the high frequencies where the level is low and no clear direction is seen.

To further investigate BC power transmission through the skull interior, the power transmission pathway in Fig. 9a was computed in all three directions as the sum of the absolute value of the power through a $1 \text{ mm} \times 1 \text{ mm}$ area in the three dimension (cf. Figure 7). The result of this computation is shown in Fig. 9b. The result in Fig. 9b is very similar to the result in Fig. 9a, indicating that there is no other direction in the pathway transmitting significant amount of sound power but low frequency sound power seem to be transmitted in the brain tissue, while high-frequency power is attenuated. There is a systematic decrease in sound power magnitude at the mid- and high frequencies from the surface of the brain toward the center. One reason for this decrease is that the brain tissue is modeled as an elastic material with a frequency dependent loss factor (Chang et al. 2016). The abrupt power transmission changes close to the skull bone may be a result of the impedance mismatch between the stiff skull bone and the elastic brain tissue leading to a large reflection of power at the boundary.

4 Discussion

In the current study, the vibratory power in the skull and the dominant pathways of BC sound power transmission were investigated when stimulation was at the mastoid. The results were obtained by simulations of the LiUHead, a FE model of a female human head.

The FE model was described in Chang et al. 2016. Even if this type of model enables analysis of BC sound transmission, it has limitations. First, even if the LiUHead was validated against experimental data of human heads (Chang et al. 2016), the model is a simplification and does not comprise all details of a real head. Second, the results were all based on BC sound stimulation at the mastoid, directly attached to the skull bone. The power conduction and pathways would be different if the stimulation was at another position or onto the skin. Third, the measurement positions around the stimulation position were limited. If a finer mesh had been used, slightly different pathway directions could have been obtained. Also, the simulations were done in one head, and the results may be different in another head with a different anatomy and geometry. Moreover, the FE solver has its own limitation. Except the influences of the mesh, the calculations are based on numerical iterations and there is always a small uncertainty of the outcome. However, the relative tolerance in the current computations was 0.001, which means that the noise in the simulations at a frequency is more than 30 dB below the signal for energy calculations (better than 60 dB SNR for the amplitude). This is far better than

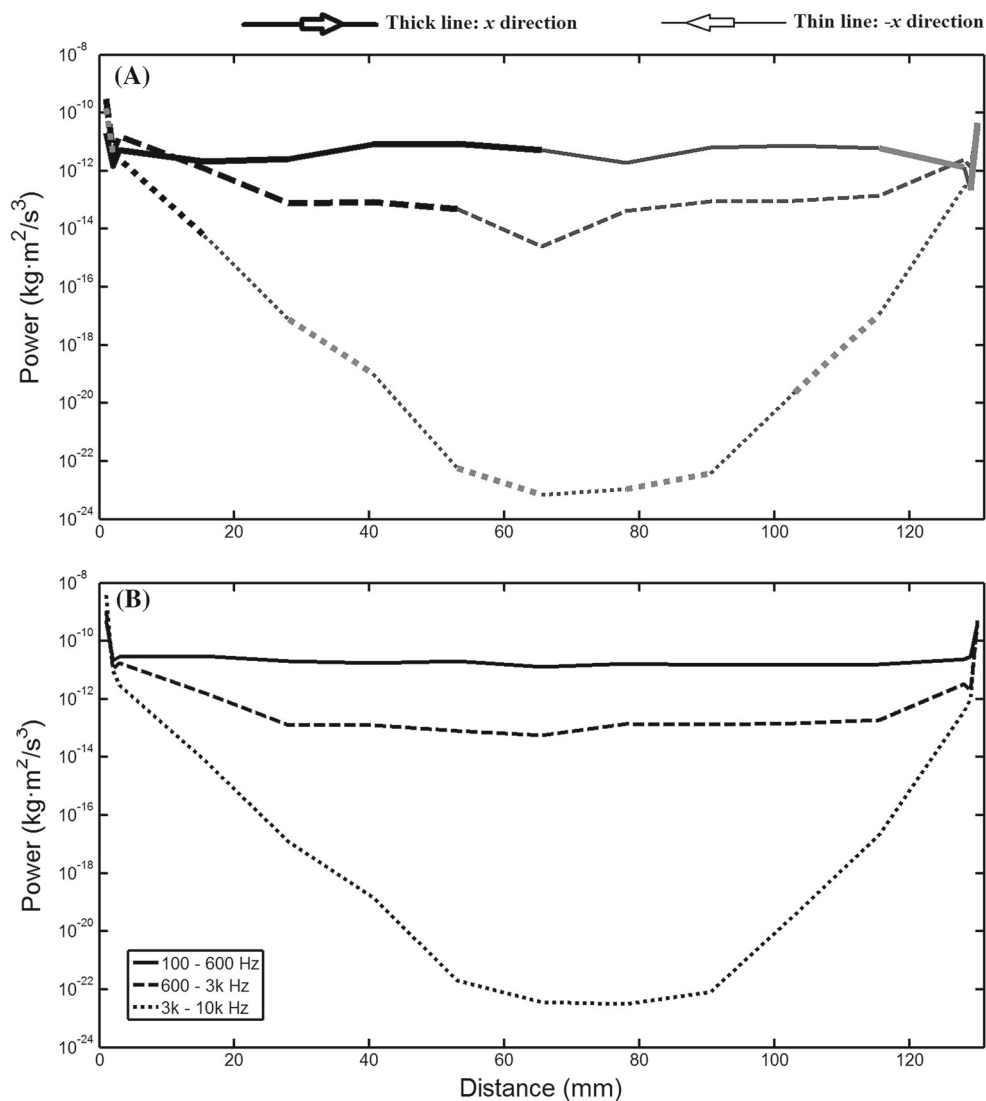


Fig. 9 **a** The power transmitted in a pathway between the middle of the two boundaries between the skull bone and the brain in Fig. 2. The outermost positions are at the skull bone to CSF boundary, the next position in the CSF (1–2 mm from the endpoints) and then the positions are inside the brain tissue. The thick lines indicate power transmission in the x -direction (Fig. 2), and thin lines indicate power transmission opposite to the x -direction which is illustrated with arrows in the top

of figure. Low frequencies (100–600 Hz) are shown with a solid line, mid-frequencies (600–3 kHz) with a dashed line, and high frequencies (3–10 kHz) with a dotted line. **b** same as (a) but the power is computed as the sum of the transmitted power in all three dimension. There is no direction of the power transmission in (b), and all lines have the same linewidths

the typically 10–20 dB SNRs that is obtained in experimental investigations on BC sound in the human. However, there is no guarantee that the results obtained here are not affected by computational noise but overall tendencies are believed to reveal important information about BC sound transmission in the human.

4.1 Power dissipation

The law of energy conservation means that in a steady state condition, as in the current simulations, all power supplied

into the system needs to dissipate. This dissipation is shown for the three structures in Fig. 4 when the stimulation is at the mastoid. The simulation was done in a free boundary condition, and no impedances were acting on the head affecting the vibrations. This is different from a normal situation where the head is situated in air and power can be transmitted out from the system as radiated sound. Instead, the loss of power in the structure was through heat conversion based on the loss factors of the different structures.

If the head were positioned in air, some vibratory power would be transferred to acoustic sound due to the interaction

of the head surface motion and the air. Since the head was not simulated in air, it is not possible to know how much this would affect the vibrations of the head and the power flows in the different structures. As a rough estimate of the radiated power (P_{AirRad}), the velocity normal to the surface of the head (v_s) was extracted and multiplied with impedance of air (Z_0) and integrated over the entire head surface according to

$$P_{\text{AirRad}} = 0.5 \cdot \int_{\text{Surface}} \text{real}(Z_0 \cdot v_s \cdot v_s^*) \quad (5)$$

In these computations, an acoustic impedance of 410 Pa*s/m was used and the total surface area was 0.142 m². According to these computations, the acoustic radiated power is between 10^{-4} and 10^{-3} of the total input power up to 500 Hz, between 10^{-3} and 10^{-2} of the total input power between 0.5 and 4 kHz, and, above 4 kHz, falling with frequency to 10^{-4} of the total input power at 10 kHz. Consequently, the power radiated as sound into the air is at most 1% of the total power dissipated in the head, and it not being included in the current simulations gives negligible effects on the result.

4.2 Power flow

When the BC power flow in the head was calculated, the skull base and occipital bone of the skull dominated the power flow throughout the investigated frequency range. Most studies of BC sound transmission only include the vibration of the skull bone (Eeg-Olofsson et al. 2008; Eeg-Olofsson et al. 2011; Eeg-Olofsson et al. 2013; Håkansson et al. 1986; Stenfelt and Goode 2005a; von Békésy 1932). However, BC power flows in other tissues, as Fig. 4 illustrates. There is limited information about the amount of sound transmitted in either the soft tissues outside of the skull bone or in the brain tissue inside the skull bone. In a study by Stenfelt et al. (2003), the ear canal sound pressure with BC stimulation was dominated by the sound radiation from the soft tissue and cartilage part of the ear canal for frequencies up to at least 2 kHz. In another study, the ear canal sound volume velocity from BC sound from the soft tissue and cartilage part of the ear canal was modeled to be 6 times greater than that from the bony part at 1 kHz, with increasing importance at lower frequencies and decreasing importance at higher frequencies (Stenfelt and Reinfeldt 2007). Neither of those studies gave an estimate of the vibration transmitted in the soft tissues, but indicated that the vibration transmission in the soft tissues diminish with frequency compared to the skull bone vibration transmission. This is in line with the simulations of sound power presented in Fig. 4 showing the soft tissues to transmit vibratory power at the low frequencies (500 Hz) but decreasing with frequency.

Ganpule et al. (2013) reported the relationship between the surface pressure on the soft tissue and the cranial and

intracranial stress in a dummy head in the area of brain injury research. Those results showed that the surface pressure was around twice the intracranial stress, but the cranial bone stress was close to one order of magnitude greater than the surface pressure. Although these simulations were conducted in the time domain with blast excitation and the outcome was the pressure, the results indicated that the sound pressure in the skull bone is much higher than in the soft tissues or skull interior, which was also found for a stationary analysis of the power flow in Fig. 4.

The skull interior is normally not considered important for BC hearing. Here, it was found that the power flow in Fig. 4 was significantly less in the skull interior than in the skull bone and the soft tissues. It has been suggested that the skull interior may be one important contributor to BC hearing in the human (Sohmer et al. 2000) and sound pressure inside the brain during BC excitation has been reported (Roosli et al. 2016; Sim et al. 2016). The current simulations indicate that sound power flows inside the brain tissue exist during BC stimulation but at a significant lower magnitude than in the skull bone. Even so, the simulation results cannot predict the importance of the intracranial sound power for hearing BC sound.

The cross-sectional plots of the power flow distribution in Fig. 4 showed that at low frequencies, the distribution of the power flow is more widespread over the entire volume while at mid- and high frequencies, the power flow is mostly concentrated close to the stimulation position. Figure 4 also revealed that the power flow in the skull bone is greater than in the other two structures. It is further illustrated that the BC power flow in the skull bone is concentrated to the skull base and back of the head when the stimulation is at the mastoid, and relatively small amounts of BC power flow is found at the vertex and at the front of the head.

4.3 Directions of the power transmission in the skull bone

The transcranial BC sound transmission has been investigated by several authors (Eeg-Olofsson et al. 2013; Stenfelt and Goode 2005a; Stenfelt 2011; Stenfelt 2012) but without discussions about the BC pathways or directions of the transcranial transmission. Another reported measure was the contralateral cochlear vibration response with multiple stimulation positions in dry skulls (Stenfelt et al. 2000), cadaver heads (Eeg-Olofsson et al. 2008; Eeg-Olofsson et al. 2011; Stenfelt and Goode 2005a), or live humans (Eeg-Olofsson et al. 2013). Those experiments could, to a certain extent, indicate the directions and pathways of BC sound transmission. The cadaver head studies have indicated that the vibration response of the contralateral cochlea is relatively insensitive to the exact stimulation position at the ipsilateral side. This indicates that the vibration transmission pathways

are similar irrespective of the exact stimulation position. In the current simulation study, only one stimulation position was used, but according to the above, the current results are not specific to the stimulation position used but can be generalized to any stimulation position at the ipsilateral mastoid. Moreover, it was suggested in Stenfelt and Goode (2005b) that the skull base was more efficient at transmitting the BC sound to the ipsilateral cochlea than the cranial vault. That is in line with the current finding where the main BC sound power flow in the skull bone was found at the skull base (Figs. 4 and 5).

Compared with real humans, the current model lacks the connection of the head to the neck and body. The head-neck junction could impede the vibration at the skull base and thereby diminish the importance of BC sound transmission through the skull base. However, the head-neck junction is insignificant at frequencies above 400 Hz (Stalnaker et al. 1971). Therefore, the model simulations indicate that the skull base is the most important BC transmission pathway holds for live humans except at the lowest frequencies. Similar results could also be seen in Fig. 4 where the skull base shows higher power flow than other structures at all three frequencies. Moreover, in Fig. 4, the directions through occipital bone and skull base show higher power transmission than the directions through the vertex and forehead, which is in line with the data in Fig. 5 where the radially power transmission between 3 and 4 rad are significantly greater than the radially power transmission between 0 and 2 rad.

The negative power for low and mid-frequencies at directions toward the vertex in Fig. 5 was unexpected that close to the stimulation position. This means that at some of the positions 20 mm from the stimulation position, the power transmission is toward the stimulation position. This finding can be explained by the vibration modes of the skull at lower frequencies (Stenfelt 2011). At these frequencies, the skull motion can be approximated with that of a rigid body with translational and rotational motion. One rotational axis would be from the center of the occiput to the nose, and this rotational motion would lead to a radially out-of-phase motion in the skull bone from the stimulation position and toward the vertex, while it would lead to an in-phase motion from the stimulation position toward the skull base. Consequently, the low-frequency out-of-phase motion is believed to be, at least partly, responsible for the negative power seen in Fig. 5.

The three pathways identified in Fig. 5 and investigated in Figs. 6 and 7 were between the stimulation position and the corresponding position at the contralateral side, according to the transmission directions (Fig. 5). These pathways are imaginary, and it is not suggested that this is the only way the BC sound is transmitted from one side to the other, as also indicated in Fig. 4. However, it gives an indication of how the BC sound power alters from one side to the other. Moreover,

Fig. 4 suggests that the BC sound power flow in the skull base is relatively homogenous, and pathway A can be seen as the general BC sound power transmission in the skull base. In general, the BC sound power in-line with the pathway direction decreases with distance and the rate of decrease is greater at high than at low frequencies (Fig. 6). The power level fluctuates at positions at the back of the head, which is seen in the logarithmic scaling in Fig. 7 for pathways B and C. The reason for these deflections seems to be unrelated to the alteration of the skull bone thickness (area shown in Fig. 6). It might be caused by the curvature of the skull, which results in power flux perpendicular to the pathway direction. When the transmitted power along the direction of the pathways for all frequencies is compared with the overall transmitted power in all directions in Fig. 7, the overall transmitted power (dashed lines in Fig. 7) shows less variability with distance than the transmitted power along the direction of the pathways.

In Fig. 7, the decrease of the overall transmitted power was steep at the beginning but then slowed down and at some distances even increased. This behavior suggests that power is lost in line with the pathway for the first half of the pathway and that some BC sound power is restored in the second half. Ganpule et al. (2013) reported similar findings when investigating brain injury. When the blast was located at the front of the head, the maximum cranial pressure decreased with distance but increased when measured at the posterior fossa, opposite to the stimulation side. This finding can be explained by two mechanisms. The first mechanism is the spread and refocus of the power. If the skull is approximated by the surface of a sphere, the surface vibrations around the stimulus position spread in arcs with wave fronts that form expanding circles on the head surface until the vibrations cover half of the sphere. At that point, the circular wave fonts begin to collapse and are refocused at a point on the opposite side of the head from the stimulus. If no power is lost, all power would be refocused on the position opposite to the stimulation position. Even if the skull is not a perfect sphere, it has a sphere-like geometry and the power is expected to increase at the opposite side due to the above explained phenomenon. The second mechanism is the transfer of power from the skull bone to the skull interior that is transferred back to the skull bone on the contralateral side. This mechanism will be discussed in the next section.

Even if the three pathways have different starting points and distances, the overall transmitted powers in Fig. 7 show approximately 15 dB transcranial attenuation between the stimulation side and the contralateral side for all three pathways (1.5 orders of magnitude). In a study on transcranial transmission in live humans, Håkansson et al. (1994) applied vibration on a titanium screw in the skull bone intended for bone conduction hearing aids and measured the vibration on a similar screw at the contralateral side. The screws in the study of Håkansson et al. (1994) were attached approx-

imately 55 mm behind the ear canal opening, a position approximately 35 mm posterior to the stimulation position in the current study. They reported an average transcranial loss of about 13 dB, a level similar to the simulation results here. Other studies of the transcranial transmission have often reported no or little attenuation up to 1 kHz and an increase in attenuation amounting to approximately 10–20 dB at 10 kHz (Eeg-Olofson et al. 2011; Stenfelt and Goode 2005a, b; Stenfelt 2012). However, those studies estimate the BC sound difference between the two cochleae that is different from the study here where the transcranial transmission is estimated between two positions on the mastoid of the cranium (see Fig. 2).

4.4 Transmission through the skull interior

As indicated in the previous section, the BC sound may be transmitted through the skull interior to the contralateral side. The study by Freeman et al. (2000) on experimental animals suggested that a major pathway involved in the transmission of BC sound power from the site of bone vibrator application on the skull to the inner ear is via the tissues in the cranial space. Experimental results in humans by Sohmer et al. (2000) also reported that BC sound power from a vibration transducer applied directly to the dura caused sound perception which was attributed to sound transmission through the CSF. Moreover, experiments in human cadaver heads have shown that there is a sound pressure inside the skull during BC stimulation (Roosli et al. 2016; Sim et al. 2016), but it was estimated not to be important for BC hearing in the human with a normal functioning ear (Stenfelt 2016). However, it is not clear how the BC sound in the skull bone and skull interior interacts. Therefore, the interaction between ipsilateral and contralateral skull bone and skull interior was investigated here at a position that did not involve the stimulation position (Fig. 2). If the stimulation position was involved, as the results in Fig. 8 show, BC sound power is transmitted from skull bone to the skull interior. However, when investigating the BC sound transferred between the skull bone and the skull interior at an interface excluding the stimulation position, the interaction between the skull bone and the brain and CSF was significantly less.

Figure 8 suggests that the sound power is transmitted from the ipsilateral skull bone to the contralateral skull bone through the skull interior at the higher frequencies (power fluxes positive at both sides in Fig. 8). However, Fig. 9 shows that there is no effective sound power transmission through the skull interior at high frequencies, neither in-line with the transmission direction (Fig. 9a) nor in all space dimensions (Fig. 9b). Consequently, the power transmission between the skull bone and the skull interior seems to be local. The power flow is shown for the brain in Fig. 4, and it indicates a large power flow magnitude difference between the skull bone and

the brain, so from that result, the rapid decline in power transmission from the skull bone to the brain tissue was to be expected. There is a thin layer of CSF between the skull bone and the brain, and the power exchange between the skull bone and skull interior seems to be limited to this small layer. One hypothesis is that when the BC sound travels in the skull bone as transverse or bending wave motion at the higher frequencies (Stenfelt and Goode 2005b), this wave motion causes fluid to move tangential to the skull in the opposite direction of the wave motion, inducing a power exchange between the skull bone and the CSF. However, this hypothesis needs to be investigated further to reveal the nature of the vibratory power exchange between the skull bone and skull interior.

The drastic reduction of power transmission through the brain at higher frequencies should be interpreted cautiously. The model uses a frequency dependent attenuation of the sound transmission in the brain tissue, which may overestimate the reduction of power transmission in the brain. Moreover, the mesh of the brain in the LiUHead is not as fine as the other parts, and the power transmission results for the brain are less reliable than those obtained in other parts of the LiUHead. However, even if the power transmission data in the brain is less reliable than the power transmission data obtained in the skull bone, the results in Fig. 9 indicate that the power transmission through the brain is of minor importance for BC sound transmission.

5 Conclusions

In this study, BC sound was simulated in a human head using a validated FE model to investigate the BC sound power transmission. The simulations indicate that the skull bone dominates the BC sound power transmission and that the greatest power flow is concentrated to the stimulation position. With a stimulation force of 1 N, the highest sound power dissipation in the skull bone was found at the highest frequencies. The overall findings are in line with the general assumption that the skull bone is the most important media for BC sound, hence its name. The soft tissue covering the skull bone is the second most important media, and the skull interior is the least important media for BC sound power transmission.

When the vibration force is applied at the mastoid, the transmission of BC sound power in the skull is mainly concentrated to the skull base, closed to the foramen magnum. In addition, BC sound power is transmitted through the occipital bone. Relatively little power is transmitted over the vertex or forehead, and at low and mid-frequencies, the power seem to be in the direction from the vertex toward the stimulation position. Overall, the BC power flow in the skull bone decreases with distance from the excitation point. The high-frequency BC power flow declines more rapidly with distance

than the mid- and low-frequency BC power flow which is in line with experimental findings. The simulation indicates that there is BC sound power transfer between the skull bone and the skull interior, but the neural tissues seem not to transmit BC sound power at mid- and high frequencies. The interaction between skull bone and skull interior is only local and does not involve BC sound transmission through the brain. This suggests that BC sound is not transmitted through the skull interior, but the major part of the sound power transmitted to the contralateral side is transmitted in the skull bone.

Acknowledgements The FE model was supported by the European Union under Grant No. 600933 for the SIFEM project.

Compliance with ethical standards

Conflict of interest We declare that we have no financial and personal relationships with other people or organizations that can inappropriately influence our work, there is no professional or other personal interest of any nature or kind in any product, service and/or company that could be construed as influencing the position presented in, or the review of, the manuscript entitled, The FE model was supported by the European Union under Grant No. 600933 for the SIFEM project.

Open Access This article is distributed under the terms of the Creative Commons Attribution 4.0 International License (<http://creativecommons.org/licenses/by/4.0/>), which permits unrestricted use, distribution, and reproduction in any medium, provided you give appropriate credit to the original author(s) and the source, provide a link to the Creative Commons license, and indicate if changes were made.

References

- Békésy GV (1932) Zur theorie des hörens bei der schallaufnahme durch knochenleitung. *Ann Phys* 405:111–136
- Berger KW (1976) Early bone conduction hearing aid devices. *Arch Otolaryngol* 102:315–318
- Chang Y, Kim N, Stenfelt S (2016) The development of a whole-head human finite-element model for simulation of the transmission of bone-conducted sound. *J Acoust Soc Am* 140:1635–1651
- Dobrev I, Sim JH, Stenfelt S, Ihrle S, Gerig R, Pfiffner F, Eiber A, Huber AM, Röösli C (2017) Sound wave propagation on the human skull surface with bone conduction stimulation. *Hear Res* 355:1–13
- Eeg-Olofsson M, Stenfelt S, Tjellström A, Granström G (2008) Transmission of bone-conducted sound in the human skull measured by cochlear vibrations. *Int J Audiol* 47:761–769
- Eeg-Olofsson M, Stenfelt S, Granström G (2011) Implications for contralateral bone-conducted transmission as measured by cochlear vibrations. *Otol Neurotol* 32:192–198
- Eeg-Olofsson M, Stenfelt S, Taghavi H, Reinfeldt S, Håkansson B, Tengstrand T, Finizia C (2013) Transmission of bone conducted sound—correlation between hearing perception and cochlear vibration. *Hear Res* 306:11–20
- Freeman S, Sichel J-Y, Sohmer H (2000) Bone conduction experiments in animals—evidence for a non-osseous mechanism. *Hear Res* 146:72–80
- Ganpule S, Alai A, Plougonven E, Chandra N (2013) Mechanics of blast loading on the head models in the study of traumatic brain injury using experimental and computational approaches. *Biomech Model Mechanobiol* 12:511–531
- Håkansson B, Carlsson P, Tjellström A (1986) The mechanical point impedance of the human head, with and without skin penetration. *J Acous Soc Am* 80:1065–1075
- Håkansson B, Brandt A, Carlsson P, Tjellström A (1994) Resonance frequencies of the human skull in vivo. *J Acoust Soc Am* 95:1474–1481
- Hambric SA (1990) Power flow and mechanical intensity calculations in structural finite element analysis. *J Vib Acoust* 112:542–549
- Lee JS (1980) Digital image enhancement and noise filtering by use of local statistics. *IEEE Trans Pattern Anal Mach Intell* 2:165–168
- Mudry A, Tjellström A (2011) Historical background of bone conduction hearing devices and bone conduction hearing aids. *Implantable bone conduction hearing aids*, vol 71. Karger Publishers, Basel, pp 1–9
- Roosli C, Dobrev I, Sim JH, Gerig R, Pfiffner F, Stenfelt S, Huber AM (2016) Intracranial pressure and promontory vibration with soft tissue stimulation in cadaveric human whole heads. *Otol Neurotol* 37:e384–e390
- Sim J, Dobrev I, Gerig R, Pfiffner F, Stenfelt S, Huber A, Röösli C (2016) Interaction between osseous and non-osseous vibratory stimulation of the human cadaveric head. *Hear Res* 340:153–160
- Sohmer H, Freeman S, Geal-Dor M, Adelman C, Savion I (2000) Bone conduction experiments in humans—a fluid pathway from bone to ear. *Hear Res* 146:81–88
- Stalnaker RL, Fogle JL, McElhaney JH (1971) Driving point impedance characteristics of the head. *J Biomech* 4:127–139
- Stenfelt S (2011) Acoustic and physiologic aspects of bone conduction hearing. *Implantable bone conduction hearing aids*, vol 71. Karger Publishers, Basel, pp 10–21
- Stenfelt S (2012) Transcranial attenuation of bone-conducted sound when stimulation is at the mastoid and at the bone conduction hearing aid position. *Otol Neurotol* 33:105–114
- Stenfelt S (2013) Bone conduction and the middle ear. The middle ear. Springer, Berlin, pp 135–169
- Stenfelt S (2016) Model predictions for bone conduction perception in the human. *Hear Res* 340:135–143
- Stenfelt S, Goode RL (2005a) Transmission properties of bone conducted sound: measurements in cadaver heads. *J Acoust Soc Am* 118:2373–2391
- Stenfelt S, Goode RL (2005b) Bone-conducted sound: physiological and clinical aspects. *Otol Neurotol* 26(6):1245–1261
- Stenfelt S, Reinfeldt S (2007) A model of the occlusion effect with bone-conducted stimulation. *Int J Audiol* 46:595–608
- Stenfelt S, Hato N, Goode RL (2002) Factors contributing to bone conduction: the middle ear. *J Acoust Soc Am* 111:947–959
- Stenfelt S, Håkansson B, Tjellström A (2000) Vibration characteristics of bone conducted sound in vitro. *J Acoust Soc Am* 107(1):422–431
- Stenfelt S, Wild T, Hato N, Goode RL (2003) Factors contributing to bone conduction: the outer ear. *J Acoust Soc Am* 113:902–913
- Structural Mechanics Module Users Guide, Chapter 3, p 410

Publisher's Note Springer Nature remains neutral with regard to jurisdictional claims in published maps and institutional affiliations.